Infrared photoresistance as a sensitive probe of electronic transport in twisted bilayer graphene

2D Materials

OPEN ACCESS

RECEIVED
28 July 2022

REVISED
7 October 2022

ACCEPTED FOR PUBLICATION
17 October 2022

PUBLISHED
3 November 2022

PAPER

Infrared photoresistance as a sensitive probe of electronic transport in twisted bilayer graphene

S Hubmann[1], G Di Battista[2,3], I A Dmitriev[1], K Watanabe[4], T Taniguchi[5], D K Efetov[2,3,6] and S D Ganichev[1,7,*]

[1] Terahertz Center, University of Regensburg, 93040 Regensburg, Germany
[2] ICFO—Institut de Ciencies Fotoniques, The Barcelona Institute of Science and Technology, Castelldefels, Barcelona 08860, Spain
[3] Fakultät für Physik, Munich Quantum Center, and Center for NanoScience (CeNS), Ludwig-Maximilians-Universität München, Geschwister-Scholl-Platz 1, 80539 München, Germany
[4] Research Center for Functional Materials, National Institute for Materials Science, 1-1 Namiki, Tsukuba 305-0044, Japan
[5] International Center for Materials Nanoarchitectonics, National Institute for Materials Science, 1-1 Namiki, Tsukuba 305-0044, Japan
[6] Munich Center for Quantum Science and Technology (MCQST), Schellingstraße 4, 80799 München, Germany
[7] CENTERA Laboratories, Institute of High Pressure Physics, Polish Academy of Sciences, PL-01-142 Warsaw, Poland
[*] Author to whom any correspondence should be addressed.

E-mail: sergey.ganichev@ur.de

Keywords: photoresistance, twisted bilayer graphene, infrared, temperature, bolometric, heating

Abstract

We report on observation of the infrared photoresistance of twisted bilayer graphene (tBLG) under continuous quantum cascade laser illumination at a frequency of 57.1 THz. The photoresistance shows an intricate sign-alternating behavior under variations of temperature and back gate voltage, and exhibits giant resonance-like enhancements at certain gate voltages. The structure of the photoresponse correlates with weaker features in the dark dc resistance reflecting the complex band structure of tBLG. It is shown that the observed photoresistance is well captured by a bolometric model describing the electron and hole gas heating, which implies an ultrafast thermalization of the photoexcited electron–hole pairs in the whole range of studied temperatures and back gate voltages. We establish that photoresistance can serve a highly sensitive probe of the temperature variations of electronic transport in tBLG.

1. Introduction

In a breakthrough discovery in 2018 it was experimentally shown that when two graphene layers are stacked vertically, while being twisted by a magic angle of 1.1°, the inter-layer hybridization leads to the emergence of ultra-flat electronic bands [1–3]. Strikingly, these bands were found to host a plethora of exotic electronic phases including unconventional superconductivity, correlated insulators, as well as magnetic and topological phases [2–6]. These discoveries, demonstrating that the twist angle can be used to control the state of 2D materials and for manipulation of strong electronic correlations, produced a remarkable excitement and multidisciplinary research (see, e.g. [7–25] and references therein). In particular, optoelectronic studies provide a way to access the unique and rich physics of twisted bilayer graphene (tBLG) and open a potential for a novel kind of devices, such as detectors of terahertz and infrared radiation [26, 27]. So far, these studies have been limited to investigation of photocurrents excited in unbiased tBLG structures [22, 28–39].

Here we report on observation and study of the infrared photoresistance in tBLG with small twist angle of ∼1°. The photoresistance exhibits a complex sign-alternating behavior upon variation of the back gate voltage and the sample's temperature. In particular, at low temperatures it exhibits sharp negative spikes at several gate voltages. We show that the infrared photoresistance is caused by the bolometric effect—change of the dc resistivity due to electron and hole gas heating. This conclusion is supported by the fact that the photoresistance closely follows the first derivative of the dark dc resistance with respect to the temperature: the shape of the gate-voltage dependence of the photoresistivity at all temperatures practically coincides with the difference of resistance traces obtained at two neighboring temperatures. This property enables us to estimate the heating effect and to demonstrate its weak sensitivity both to the

measurement temperature and to the gate voltage, controlling the low-energy moiré band structure and position of the chemical potential in tBLG. We thus establish that, despite high energy of electron–hole pairs excited by the infrared radiation, the rich structure and sharp negative spikes in the gate voltage of observed photoresistance are completely determined by the temperature variations of low-energy transport, which is strongly affected by the moiré potential of small angle tBLG. Our study demonstrates that photoresistance can serve as a sensitive probe of the low-energy transport characteristics, even those that are hardly detectable using the standard transport measurements.

2. Samples and methods

The heterostructure consisting of the tBLG layer sandwiched between hexagonal boron nitride (hBN) was prepared using a 'cut and stack' technique, where a single flake of monolayer graphene is cut in two pieces using an AFM tip, and these two pieces are stacked together via substrate rotation yielding a controlled twist between the two graphene layers, for details see [40]. Bottom and top layers of hBN had a thickness of 16 and 10 nm, respectively. The two graphene sheets were stacked one on top to the other at a target angle of 1°. A graphite layer on the bottom of the hBN/tBLG/hBN was used as a local back gate electrode. The stack was etched into a Hall bar geometry $17 \times 2\,\mu\text{m}^2$. A CHF_3/O_2 mixture was used to expose the graphene edges, with subsequent evaporation of Cr/Au (5/50 nm) providing ohmic contacts for transport and photoresistance measurements.

The sample was placed in a temperature-variable He exchange gas optical cryostat with ZnSe windows. To capacitively tune the carrier density in the tBLG structure, back gate voltage U_G in the range of ± 3 V was applied to the graphite back gate of the device. The sample resistance, R, was measured in two-terminal geometry using the standard low-frequency lock-in technique, with excitation current of 100 nA.

Figure 1 shows the sample resistance as a function of the applied gate voltage measured at different temperatures in the range from $T = 3.6$ to 170 K. At low temperatures the resistance exhibits clear sharp peaks at certain gate voltages characteristic for tBLG: The charge neutrality point (CNP)-peak at $U_{G,\text{eff}} = 0$ V is flanked by highly-resistive peaks at ± 2.5 V with strongly insulating behavior. From the position of these peaks which mark the edges of the moiré bands, the twist angle was estimated to be $\sim 1°$, using the thickness of the bottom hBN layer to calculate the gate capacitance. The resistance traces also show less pronounced peaks at ± 1 V. This suggests that the area between the source and drain contacts B and C (see figure 2) acquires some twist angle inhomogeneity, i.e. that the measured area is dominated by a twist angle of $\sim 1°$ but also contains fractions with lower twist angles of $\sim 0.6°$. Recent studies with STM or SQUID-on-tip techniques [19] provide a direct experimental evidence of such twist angle inhomogeneity. The inhomogeneity can also be responsible for the double-peak structure of R at ± 2.5 V. Note that the gate voltage corresponding to the CNP, U_{CNP}, was varying slightly between different sample cooldowns due to different charge trapping in the gate insulator [41, 42]. Correspondingly, in the presented data we use the effective gate voltage $U_{g,\text{eff}} = U_G - U_{CNP}$.

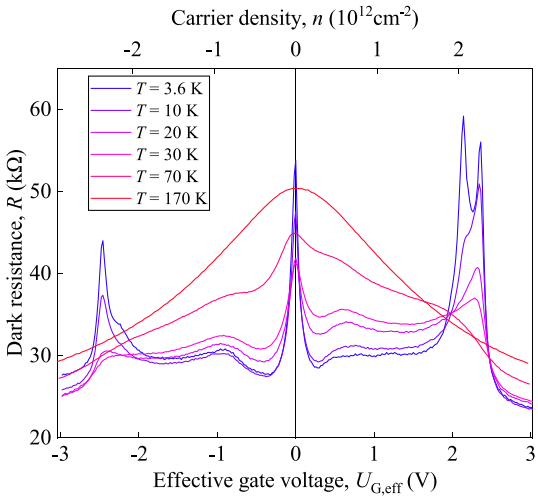

Figure 1. Two-point dc resistance R measured between contacts B and C (see inset in figure 2) as a function of the effective gate voltage at temperatures T ranging from 3.6 to 170 K. The upper axis shows the corresponding carrier density calculated using the gate capacitance as $n = U_{G,\text{eff}} \cdot 9.62 \times 10^{11}\,\text{V}^{-1}\,\text{cm}^{-2}$.

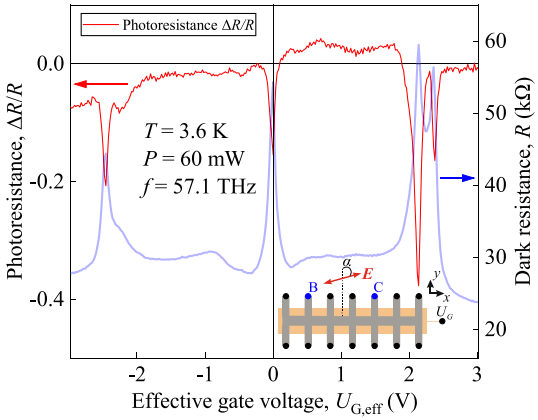

Figure 2. Normalized photoresistance $\Delta R/R$ as a function of the effective gate voltage at a temperature $T = 3.6$ K. The corresponding resistance without illumination is illustrated by blue line. The inset shows a sketch of the Hall bar structure, contacts B and C used for the two-point measurements, and the linear polarization angle with respect to the short side of the Hall bar (the azimuth angle $\alpha = 75°$).

In order to measure the photoresistance we used a continuous wave (cw) quantum cascade laser (QCL) which operated at a radiation frequency of 57.1 THz (photon energy of 236 meV) and provided an maximum output power of 130 mW. The normally incident radiation was focused onto the tBLG sample using a parabolic mirror, which resulted in a laser spot with diameter of about 0.5 mm as checked by a pyroelectric camera [43, 44]. This spot diameter was an order of magnitude larger than the Hall bar size ensuring a uniform illumination of the sample. The polarization state of the incoming radiation was controlled using a quarter-wave plate and linear polarizers. The photoresistance was measured as the difference between the two-point dc resistance in the presence and absence of cw QCL illumination, $\Delta R = R_{\rm ill} - R$. In all figures apart from figures 5 and 6, we present the results for the normalized photoresistance $\Delta R/R$.

3. Results

Applying the infrared radiation to the tBLG structure we observed a photoinduced change ΔR of the sample resistance [45]. Figure 2 shows a typical example of recorded ΔR, normalized to the dark resistance R, as a function of the applied gate voltage $U_{\rm G,eff}$. These data were obtained at the lowest $T = 3.6$ K. Besides a primary narrow negative spike at the CNP, the photoresistance $\Delta R/R$ exhibits several spikes at large negative and positive gate voltage, namely, at $U_{\rm G,eff} = -2.46$, $U_{\rm g,eff} = 2.14$, and 2.38 V. Comparison of these data with the dark resistance, see blue line in figure 2, shows that positions of the negative spikes in $\Delta R/R$ coincide with the peak positions in R. We thus observe that, despite the huge photoexcitation energy of 236 meV, the major sharp features in the $U_{\rm G,eff}$-dependence of $\Delta R/R$ correspond to the abrupt changes of dc transport properties when the chemical potential is passing the edges of the low-energy moiré bands at ∼10 meV from the CNP, see discussion below. This establishes that the infrared photoresistance can indeed serve a sensitive probe of the low-energy dc transport of tBLG. In this connection, it is worth mentioning that variations of the photoresistance ΔR with $U_{\rm G,eff}$ are orders of magnitude stronger than those in the dark resistance R (not exceeding 50%), and thus remain equally strong if the photoresistance ΔR is not normalized to the dark resistance R, see figure 5.

As the temperature of measurements increases, the behavior of the photoresistance changes substantially, see figure 3. While the photoresistance dips at positions of the peaks in dark resistance remain pronounced up to 70 K, their magnitude is significantly reduced with increasing T. These changes are again consistent with evolution of the dc resistance R in figure 1, where all peaks become progressively weaker

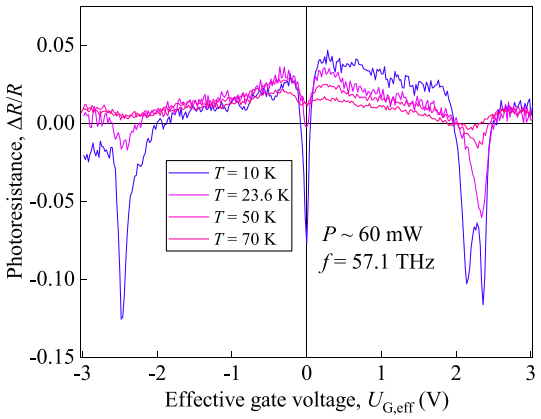

Figure 3. Normalized photoresistance $\Delta R/R$ as a function of the effective gate voltage at different temperatures from 10 to 70 K.

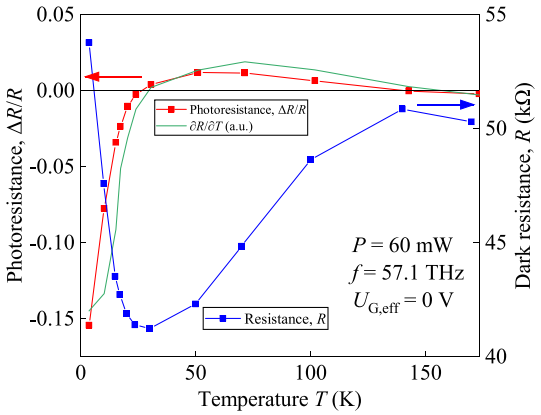

Figure 4. Temperature evolution of normalized photoresistance $\Delta R/R$ (red), resistance R (blue), and the derivative of the resistance with respect to the temperature $\partial R/\partial T$ (green) at an effective gate voltage of $U_{\rm G,eff} = 0$ V corresponding to the CNP.

and broader at elevated T (for $T \lesssim 30$ K). Moreover, one observes that the sign of ΔR at a fixed $U_{\rm G,eff}$ follows the sign of temperature variation of R at the same $U_{\rm G,eff}$, for a detailed comparison see figures 4–6. At higher T, the side peaks become very weak in R while the corresponding features are still well resolved in ΔR, whereas the broad CNP peak in R continues to broaden and starts to grow. Consistently, at $T > 70$ K the photoresistance becomes positive in the whole range of gate voltages (see figure 6(d)). Finally, for temperatures above 140 K the photoresistance signal becomes vanishingly small.

We now turn to a quantitative comparison of the temperature evolution of the dc resistance and photoresistance. Figure 4 shows the temperature dependence of the normalized photoresistance $\Delta R/R$ (red line) together with that of the resistance R without illumination (blue) at $U_{\rm G,eff} = 0$ corresponding to the CNP. It is clearly seen that

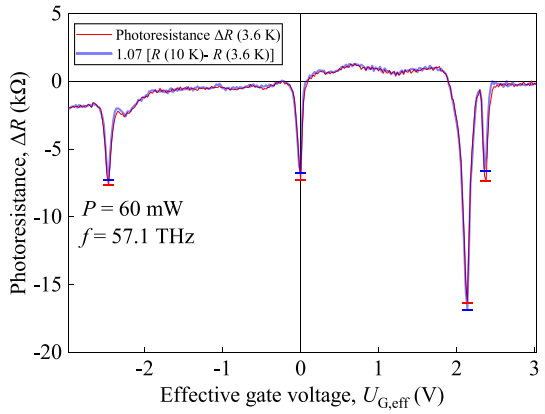

Figure 5. Photoresistance ΔR as a function of the effective gate voltage measured at a temperature of $T = 3.6$ K plotted together with the scaled difference between the dark resistances measured at $T = 10$ K and $T = 3.6$ K.

the photoresistance changes its sign with increasing temperature. Apart from that, comparing the temperature dependence of the photoresistance with the dark resistance we find that the photoresistance closely follows the temperature derivative of the dark resistance, $\partial R/\partial T$, see green line in figure 4. As discussed below, this provides a strong evidence that the observed photoresistance is caused by the radiation-induced electron and hole gas heating. Another justification comes from the analysis in figure 5. Here we directly compare the non-normalized photoresistance ΔR measured at $T = 3.6$ K (red line) with the difference of the dark resistance traces measured at temperatures of 10 and 3.6 K and observe that, up to a constant scaling factor of 1.07, these curves nearly coincide, see figure 5. Similar precise coincidence is observed at higher T, see figure 6.

4. Discussion

The results presented above demonstrate that, despite a complex moiré band structure of tBLG, the photoresistance of this material in the studied frequency range is pretty well captured by a rather common and well-established mechanism related to electron heating [46]. Within this mechanism, the stationary non-equilibrium energy distribution of electrons under continuous illumination is approximately given by the equilibrium Fermi–Dirac distribution, but with the measurement temperature T replaced by an elevated electron temperature $T_e > T$. The value of the electron temperature T_e should be found self-consistently from the energy balance equation. This equation expresses the stationary condition that, for certain $T_e > T$, the energy absorbed by electrons is fully compensated by the energy flow from hot electrons to the lattice (usually assumed to remain at the measurement temperature T). Provided $T_e - T \ll T$, the photoresistance due to electron heating is given by:

$$\Delta R = \frac{\partial R}{\partial T_e}(T_e - T), \qquad (1)$$

in full accordance with our findings, presented in figures 4–6 and discussed in more details below. This description of electron heating and of the corresponding photoresistance is generally valid when equilibration of the absorbed energy within the electron system is faster than its transfer to the thermal bath of phonons but, in practice, is also frequently applicable when this condition is violated.

In our case, the photon energy, $\hbar\omega = 236$ meV, strongly exceeds all other involved energy scales—the temperature, Fermi energy, and moiré minibands widths—all being of the order of 1 to 10 meV [2]. It follows that a typical optical absorption process takes place between occupied initial electron states well (∼120 meV) below the Fermi energy E_F and empty states well above E_F, as illustrated in the inset in figure 6(d). At such high energies the states are only weakly influenced by the moiré superlattice [27] and can be considered as a continuum without significant modulations of the density of states. Thus, a change of the gate voltage, which strongly modifies the moiré electron spectrum and resistance in the vicinity of Fermi energy and CNP, should only weakly affect the amount of absorbed energy governed by such distant states. Similarly, the relaxation of hot electrons should also possess a weak sensitivity to U_G. The photoexcited electrons and holes are expected to rapidly thermalize via electron-electron collisions simultaneously transferring the excess energy to the lattice via the acoustic phonon emission [47]. All these processes involve huge number of possible intermediate states with typical energies comparable to $\hbar\omega \gg E_F$ and, thus, may also possess a weak sensitivity to the low-energy spectrum of tBLG and the exact position of E_F, controlled by the gate voltage U_G.

As a result, the electron temperature T_e, expressing the balance between absorption and energy relaxation, is expected to be largely insensitive to U_G. In sharp contrast to T_e, the temperature derivative $\partial R/\partial T_e$ of the dark resistance should be highly sensitive to both U_G and temperature, in particular in the vicinity of the moiré band edges where the transport contributions of different states in the temperature window around the Fermi energy can be essentially different.

The above conclusions are well supported by our experimental findings, which confirm that the sign of the photoresistance correlates with the temperature dependence of R, see figure 4 [48]. Moreover, the analysis presented in figure 5 confirms that the U_G-dependence of ΔR coincides with that of $\partial R/\partial T_e$, while the electron heating factor $\Delta T \equiv T_e - T$ in equation (1) turns out to be insensitive to U_G. This

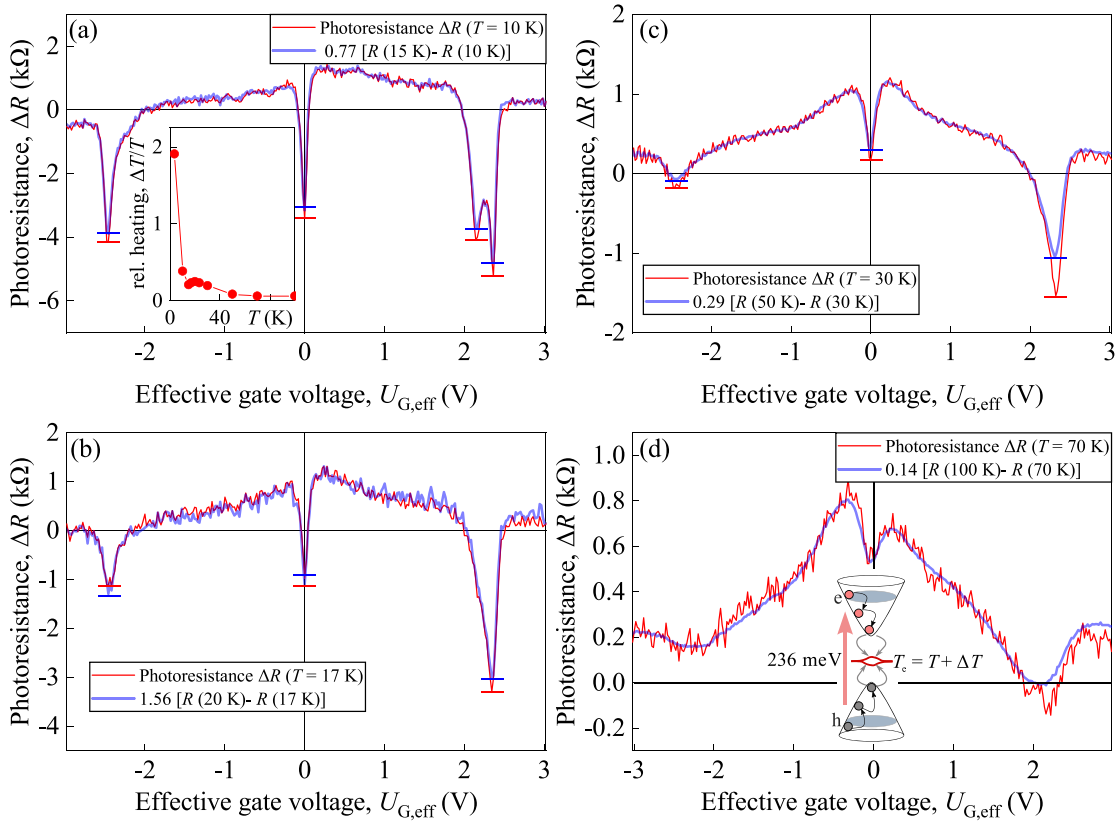

Figure 6. Photoresistance ΔR as a function of the effective gate voltage measured at temperatures of 10 K (a), 17 K (b), 30 K (c), and 70 K (d) plotted together with the scaled difference between the dark resistances measured at neighboring temperatures (provided in the legends together with the scaling factors). The inset in panel (a) shows the relative radiation-induced heating $\Delta T/T$ estimated from the scaling factors using equation (1). The inset in panel (d) shows a sketch of the optical excitation and relaxation processes leading to electron heating at energies in the vicinity of the flat bands.

implies a surprisingly low sensitivity of the high-frequency heating to the low-energy spectrum of tBLG. As discussed above, such a weak sensitivity is expected for the photoexcitation process, as well as the initial stages of thermalization and energy transfer to lattice. However, at a later stage, when the energy of nonequilibrium carriers reduces to $\sim$10 meV, one would rather expect that the relaxation process becomes sensitive to details of the band structure and position of the chemical potential. Nevertheless, our observations suggest that in the studied device the thermalization remains ultimately fast under all conditions, resulting in T_e independent of U_G.

This result is further confirmed by the analysis in figure 6: At all temperatures the shape of the photoresistance can be well reproduced by the difference of the dark resistance traces measured at two neighboring temperatures. Only in close vicinity of the strong negative spikes some small and not systematic deviations are noticeable (see horizontal bars in figures 5 and 6). These can be attributed by a limited accuracy of estimated $\partial R/\partial T$ obtained from comparison of resistance traces at two different temperatures. The scaling coefficients, obtained from such comparison (see legends in figures 5 and 6) provide an estimate for the electron heating ΔT, which remains at the level of 5 K in the whole studied interval of temperatures. From this estimate, we also establish that the relative heating $\Delta T/T$ (see inset in figure 6) remains small for all T except the lowest $T = 3.6$ K (figure 5). In the latter case equation (1), valid for the linear heating regime, is only marginally applicable, and the obtained value of ΔT can be inaccurate.

5. Summary

Summarizing, we show that, despite high energy of electron–hole pairs excited by the infrared radiation, the rich structure and sharp negative spikes in the gate voltage dependence of observed photoresistance are fully determined by the temperature variations of low-energy transport and, therefore, are strongly affected by the moiré potential of small angle tBLG. Our main observations and analysis demonstrate that photoresistance provides an alternative highly sensitive method for characterization of low-energy transport properties of tBLG which, despite its intrinsic complexity, permits a reliable treatment and clear understanding. In addition, the analysis of resistance detected in the presence and absence of radiation at varying T yields a direct access and measure of electron heating in illuminated tBLG, which may

provide an important quantitative check to future theories describing optical excitation and relaxation processes in this intriguing and rapidly developing class of 2D electronic systems.

Data availability statement

The data that support the findings of this study are available upon reasonable request from the authors.

Acknowledgments

The support from the Deutsche Forschungsgemeinschaft (DFG, German Research Foundation) via Project SPP 2244 (GA501/17-1) and Project DM1-5/1 (I A D), and from the Volkswagen Stiftung Program (97738) are gratefully acknowledged. S D G thanks the support from the IRAP program of the Foundation for Polish Science (Grant No. MAB/2018/9, Project CENTERA). D K E acknowledges support from the Ministry of Economy and Competitiveness of Spain through the 'Severo Ochoa' programme for Centres of Excellence in R and D (SE5-0522), Fundacio Privada Cellex, Fundacio Privada Mir-Puig, the Generalitat de Catalunya throughthe CERCA programme, funding from the European Research Council (ERC) under the European Union's Horizon 2020 research and innovation programme (Grant Agreement No. 852927). G D B acknowledges support from the 'Presidencia de la Agencia Estatal de Investigación' (Ref. PRE2019-088487). K W and T T acknowledge support from JSPS KAKENHI (Grant Nos. 19H05790, 20H00354 and 21H05233).

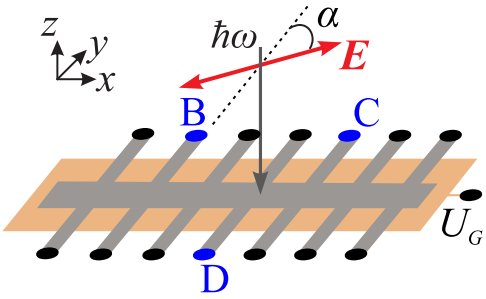

Figure 7. Sketch of the sample structure. The azimuth angle α is defined between the vector of the radiation electric field $\boldsymbol{E}$ and the short side of the Hall bar. Photosignals and transport were measured using the contacts marked in blue.

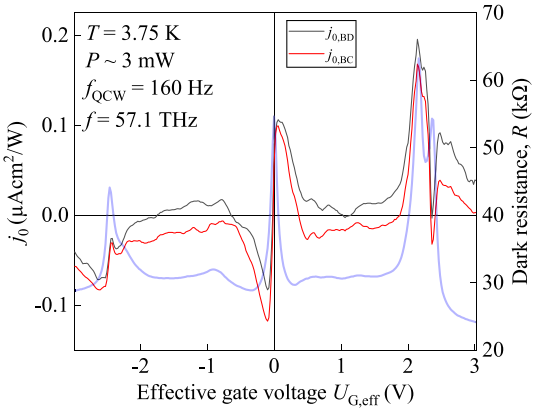

Figure 8. The gate voltage dependencies of polarization-independent component j_0 of the photocurrent, see equation (2), measured using contact pairs BC and BD. Blue line: dark resistance measured between the contacts B and C.

Appendix. Infrared radiation-induced photocurrents

Apart from the photoresistance studied in a biased tBLG, in the absence of external bias we observed polarization-dependent photocurrents. Exemplary results, obtained at low $T = 3.6$ K, are shown in figures 8–10. For the photocurrent measurements the continuous infrared 57.1 THz radiation produced by QCL was electronically modulated at a frequency of $f_{QCW} = 160$ Hz. The photocurrent along and across the Hall bar was measured using standard lock-in technique as a voltage drop between different pairs of contacts BC and BD, see figure 7.

In the case of linear polarization and low intensity I, the photocurrent $j \propto I$ can be generally represented as [22]:

$$j = j_0 - j_1 \cos(2\alpha) - j_2 \sin(2\alpha), \qquad (2)$$

where the components j_0, j_1, and j_2 are coefficients in front of the first three Stokes parameters, and the azimuth angle α is defined as the angle of linear polarization with respect to y-direction across the Hall bar, see figure 7. The last linearly independent component of the photocurrent j_C, proportional to the forth Stokes parameter, requires application of the circularly polarized radiation, in which case the second and third Stokes parameters vanish, and:

$$j = j_0 + j_C \eta. \qquad (3)$$

The helicity-dependent photocurrent contribution $j_C\eta$, proportional to the radiation helicity $\eta = \pm 1$, has opposite signs for the right- and left-handed circularly polarized radiation.

Figure 8 shows the extracted polarization-independent contribution of the photocurrent j_0 as a function of the applied gate voltage for both measurement directions BC and BD. It is seen that the photocurrent behaves similarly for both measurement directions. Similar to the photoresistance presented in the main text, the photocurrent shows pronounced features corresponding to peaks in the sample resistance (blue line in figure 8). However, in contrast to the photoresistance, at the CNP the photocurrent changes sign, together with the change of the charge of the majority carriers. Empirically,

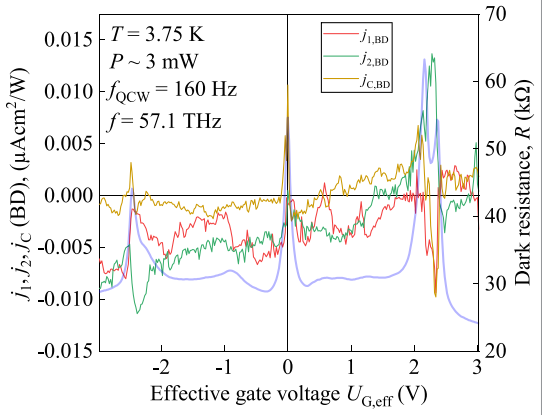

Figure 9. The gate voltage dependencies of polarization-sensitive photocurrent components j_1, j_2, and j_C, see equations (2) and (3), measured between contacts B and D. Blue line: dark resistance measured between the contacts B and C.

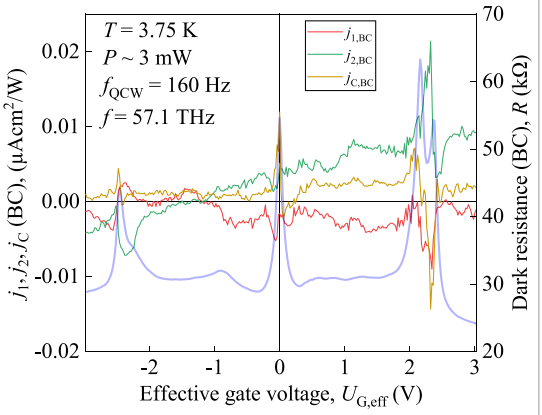

Figure 10. The gate voltage dependencies of polarization-sensitive photocurrent components j_1, j_2, and j_C, see equations (2) and (3), measured between contacts B and C. Blue line: dark resistance measured between the contacts B and C.

this behavior resembles a derivative of the resistivity with respect to the gate voltage, the density, or the Fermi energy. A similar differential line shape of the photocurrent in systems with a CNP-like feature has been reported and understood in previous works where a wide range of effects like plasmonic resonances in a Dyakonov-Shur configuration [49], thermoelectric effects [50, 51], ratchet effects [52], and edge photocurrents [42, 53] were studied.

The differential line shape has already been observed also in tBLG in the terahertz range of radiation frequencies [22, 33], where, however, it was rather linked to asymmetric scattering and the change of the carriers type at the CNP. We believe that in our device the origin is similar to that identified in [22] and is rooted in asymmetric elastic scattering of carriers. At the same time, the theory developed in [22] describes photocurrents induced via the intraband terahertz absorption, and thus is not directly applicable to the present case of direct interband transitions induced by the infrared illumination. Investigation of the corresponding mechanisms of sign-alternating tBLG photocurrents due to the interband absorption remains an interesting subject for future work. The focus of our present work is rather on photoresistance which, unlike photocurrent, does not require any spatial asymmetry, as the direction of current is defined by the external bias, absent in the photocurrent studies. The model that we successfully implemented for interpretation of results in the main text is not applicable to the photocurrents, as it does not include any asymmetry and thus results in vanishing photocurrent.

Figures 9 and 10 show the gate voltage dependences of the extracted photocurrent components j_1 and j_2, sensitive to the direction of the linear polarization, as well as the helicity-ensitive contribution j_C, separately for the transverse (contacts BD, figure 9) and longitudinal (contacts BC, figure 10) photocurrents. Similar to the polarization-independent component j_0, the polarization-sensitive components possess similar features for both measurement directions correlated with the peaks in the sample resistance (blue lines). In contrast to the photocurrents detected in previous studies in the terahertz frequency range [22, 33], in the infrared range the polarization-sensitive components are found to be much smaller than the polarization-independent photocurrent, see figure 8.

ORCID iDs

S Hubmann https://orcid.org/0000-0003-0789-6391
G Di Battista https://orcid.org/0000-0003-2643-0773
I A Dmitriev https://orcid.org/0000-0003-1370-6355
K Watanabe https://orcid.org/0000-0003-3701-8119
S D Ganichev https://orcid.org/0000-0001-6423-4509

References

[1] Bistritzer R and MacDonald A H 2011 *Proc. Natl Acad. Sci. USA* **108** 12233
[2] Cao Y, Fatemi V, Fang S, Watanabe K, Taniguchi T, Kaxiras E and Jarillo-Herrero P 2018 *Nature* **556** 43
[3] Cao Y *et al* 2018 *Nature* **556** 80
[4] Yankowitz M, Chen S, Polshyn H, Zhang Y, Watanabe K, Taniguchi T, Graf D, Young A F and Dean C R 2019 *Science* **363** 1059
[5] Sharpe A L, Fox E J, Barnard A W, Finney J, Watanabe K, Taniguchi T, Kastner M A and Goldhaber-Gordon D 2019 *Science* **365** 605–8
[6] Serlin M, Tschirhart C L, Polshyn H, Zhang Y, Zhu J, Watanabe K, Taniguchi T, Balents L and Young A F 2020 *Science* **367** 900–3
[7] Andrei E Y and MacDonald A H 2020 *Nat. Mater.* **19** 1265–75

[8] Törmä P, Peotta S and Bernevig B A 2022 *Nat. Rev. Phys.* **4** 528–42
[9] Song Z D and Bernevig B A 2022 *Phys. Rev. Lett.* **129** 047601
[10] Chaudhary S, Lewandowski C and Refael G 2022 *Phys. Rev. Res.* **4** 013164
[11] Jaoui A, Das I, Di Battista G, Díez-Mérida J, Lu X, Watanabe K, Taniguchi T, Ishizuka H, Levitov L and Efetov D K 2022 *Nat. Phys.* **18** 633–8
[12] Grover S *et al* 2022 *Nat. Phys.* **18** 885–92
[13] Cao Y, Rodan-Legrain D, Park J M, Yuan N F Q, Watanabe K, Taniguchi T, Fernandes R M, Fu L and Jarillo-Herrero P 2021 *Science* **372** 264–71
[14] Hao Z, Zimmerman A M, Ledwith P, Khalaf E, Najafabadi D H, Watanabe K, Taniguchi T, Vishwanath A and Kim P 2021 *Science* **371** 1133–8
[15] Wu S, Zhang Z, Watanabe K, Taniguchi T and Andrei E Y 2021 *Nat. Mater.* **20** 488–94
[16] Andrei E Y, Efetov D K, Jarillo-Herrero P, MacDonald A H, Mak K F, Senthil T, Tutuc E, Yazdani A and Young A F 2021 *Nat. Rev. Mater.* **6** 201–6
[17] Hesp N C H *et al* 2021 *Nat. Phys.* **17** 1162–8
[18] Liu X *et al* 2020 *Nature* **583** 221–5
[19] Uri A *et al* 2020 *Nature* **581** 47–52
[20] Cao Y, Chowdhury D, Rodan-Legrain D, Rubies-Bigorda O, Watanabe K, Taniguchi T, Senthil T and Jarillo-Herrero P 2020 *Phys. Rev. Lett.* **124** 076801
[21] Balents L, Dean C R, Efetov D K and Young A F 2020 *Nat. Phys.* **16** 725–33
[22] Otteneder M, Hubmann S, Lu X, Kozlov D A, Golub L E, Watanabe K, Taniguchi T, Efetov D K and Ganichev S D 2020 *Nano Lett.* **20** 7152–8
[23] Yoo H *et al* 2019 *Nat. Mater.* **18** 448
[24] Choi Y *et al* 2019 *Nat. Phys.* **15** 1174–80
[25] Lu X *et al* 2019 *Nature* **574** 653
[26] Seifert P, Lu X, Stepanov P, Durán Retamal J R, Moore J N, Fong K C, Principi A and Efetov D K 2020 *Nano Lett.* **20** 3459–64
[27] Di Battista G, Seifert P, Watanabe K, Taniguchi T, Fong K, Principi A and Efetov D 2022 *Nano Lett.* **22** 6465–70
[28] Xin W, Chen X D, Liu Z B, Jiang W S, Gao X G, Jiang X Q, Chen Y and Tian J G 2016 *Adv. Opt. Mater.* **4** 1703–10
[29] Yin J *et al* 2016 *Nat. Commun.* **7** 10699
[30] Sunku S S *et al* 2020 *Nano Lett.* **20** 2958–64
[31] Hesp N C H, Torre I, Barcons-Ruiz D, Sheinfux H H, Watanabe K, Taniguchi T, Kumar R K and Koppens F H L 2021 *Nat. Commun.* **12** 1640
[32] Sunku S S *et al* 2021 *Nat. Commun.* **12** 1641
[33] Hubmann S, Soul P, Battista G D, Hild M, Watanabe K, Taniguchi T, Efetov D K and Ganichev S D 2022 *Phys. Rev. Mater.* **6** 024003
[34] Deng B, Ma C, Wang Q, Yuan S, Watanabe K, Taniguchi T, Zhang F and Xia F 2020 *Nat. Photon.* **14** 549–53
[35] Kort-Kamp W J M, Culchac F J, Capaz R B and Pinheiro F A 2018 *Phys. Rev.* B **98** 195431
[36] Gao X G, Li X K, Xin W, Chen X D, Liu Z B and Tian J G 2020 *Nanophotonics* **9** 1717–42
[37] Wang J, Bo W, Ding Y, Wang X and Mu X 2020 *Mater. Today Phys.* **14** 100238
[38] Chen J, Liu C, Zeng Z and Li R 2022 *Phys. Rev.* B **105** 014309
[39] Zheng Z, Song Y, Shan Y W, Xin W and Cheng J L 2022 *Phys. Rev.* B **105** 085407
[40] Kim K, DaSilva A, Huang S, Fallahazad B, Larentis S, Taniguchi T, Watanabe K, LeRoy B J, MacDonald A H and Tutuc E 2017 *Proc. Natl Acad. Sci.* **114** 3364–9
[41] Dantscher K M *et al* 2017 *Phys. Rev.* B **95** 201103
[42] Candussio S *et al* 2021 *Phys. Rev.* B **103** 125408
[43] Ziemann E, Ganichev S D, Prettl W, Yassievich I N and Perel V I 2000 *J. Appl. Phys.* **87** 3843–9
[44] Drexler C *et al* 2012 *J. Appl. Phys.* **111** 124504
[45] Similar to our previous works [22, 33] (implementing much lower frequencies), in the absence of external bias we also observed polarization-dependent photocurrents. The corresponding results are presented in section appendix
[46] Ganichev S D and Prettl W 2005 *Intense Terahertz Excitation of Semiconductors* (Oxford: Oxford University Press)
[47] Note that the energy of photoexcited electrons and holes ($\sim$120 meV) is still insufficient for emission of optical phonons having higher energy of $\sim$200 meV
[48] In general, the resistance R depends on both electron and lattice temperatures, but at low T the latter dependence is expected to be weak due to the lack of thermal phonons with relevant momenta
[49] Bandurin D A *et al* 2018 *Nat. Commun.* **9** 5392
[50] Vicarelli L, Vitiello M S, Coquillat D, Lombardo A, Ferrari A C, Knap W, Polini M, Pellegrini V and Tredicucci A 2012 *Nat. Mater.* **11** 865–71
[51] Koppens F H L, Mueller T, Avouris P, Ferrari A C, Vitiello M S and Polini M 2014 *Nat. Nanotechnol.* **9** 780–93
[52] Olbrich P *et al* 2016 *Phys. Rev.* B **93** 075422
[53] Candussio S *et al* 2020 *Phys. Rev.* B **102** 045406